一般社団法人　電子情報通信学会
THE INSTITUTE OF ELECTRONICS,
INFORMATION AND COMMUNICATION ENGINEERS

信学技報
IEICE Technical Report
SANE2018-5 (2018-05)

SAVERS: SAR ATR with Verification Support Based on Convolutional Neural Network

Hidetoshi FURUKAWA

1778-2, Furuichiba, Saiwai-ku, Kawasaki-shi, Kanagawa, 212–0052 Japan
E-mail: hidetoshi.furukawa@ai4sig.org

Abstract We propose a new convolutional neural network (CNN) which performs coarse and fine segmentation for end-to-end synthetic aperture radar (SAR) automatic target recognition (ATR) system. In recent years, many CNNs for SAR ATR using deep learning have been proposed, but most of them classify target classes from fixed size target chips extracted from SAR imagery. On the other hand, we proposed the CNN which outputs the score of the multiple target classes and a background class for each pixel from the SAR imagery of arbitrary size and multiple targets as fine segmentation. However, it was necessary for humans to judge the CNN segmentation result. In this report, we propose a CNN called SAR ATR with verification support (SAVERS), which performs region-wise (i.e. coarse) segmentation and pixel-wise segmentation. SAVERS discriminates between target and non-target, and classifies multiple target classes and non-target class by coarse segmentation. This report describes the evaluation results of SAVERS using the Moving and Stationary Target Acquisition and Recognition (MSTAR) dataset.

Key words Automatic target recognition (ATR), Detection, Discrimination, Classification, Convolutional neural network (CNN), Synthetic aperture radar (SAR)

1. Introduction

In recent years, methods using convolution neural network (CNN) [1]–[4] have been successful in the classification of image recognition. Similarly, CNNs for synthetic aperture radar (SAR) automatic target recognition (ATR) have been proposed. On the Moving and Stationary Target Acquisition and Recognition (MSTAR) public dataset [5], the target classification accuracy of the CNNs [6]–[9] exceeds conventional methods (support vector machine, etc.). However, most of CNNs for SAR ATR classify target classes from a target chip extracted from SAR image but do not classify multiple targets or a target chip (or SAR image) of an arbitrary size. In addition, a CNN for target classification can output score or probability of each class as classification result, but it is difficult for a human to verify the classification result.

Figure 2a shows that the standard architecture of SAR ATR consists of three stages: detection, discrimination, and classification. Detection: the first stage of SAR ATR detects a region of interest (ROI) from a SAR image. Discrimination: the second stage of SAR ATR discriminates whether an ROI is a target or non-target region, and outputs the discriminated ROI as a target chip. Classification: the third stage of SAR ATR classifies target classes from a target chip.

In contrast, we proposed an architecture that performs detection, discrimination, and classification in a single stage (Fig. 2b). Furthermore, we proposed a CNN which inputs a SAR image of variable sizes with multi-target and outputs a SAR ATR image.

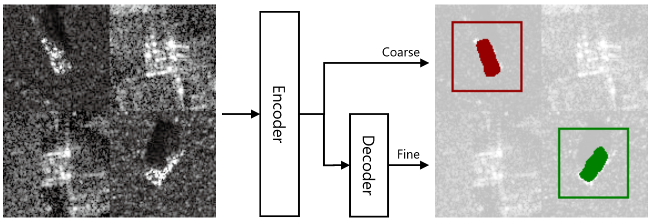

(a) Input. (b) SAVERS. (c) Output.

Fig. 1 Illustration of input and output of proposed CNN. The CNN named SAVERS performs automatic target recognition of multi-class / multi-target in variable size SAR image. In this case, the input is a single image with two targets of different classes and two clutters. SAVERS outputs the position, class, and shape of each detected target.

In this report, we propose a new CNN focusing on object detection by coarse segmentation and discrimination between target and non-target using clutter chips.

2. Related Work

In segmentation of image recognition giving classification label for each pixel of an image, methods using CNN [10]–[12] show a good performance in recent years. For SAR image, segmentation of a target region and a shadow region is

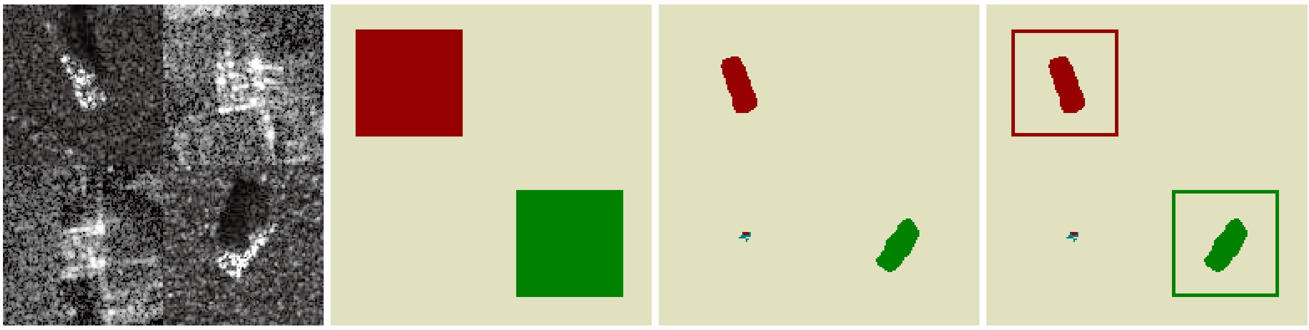

(a) Input. (b) Coarse segmentation output. (c) Fine segmentation output. (d) Composite output.

Fig. 3 Outputs of coarse segmentation, fine segmentation, and composite.

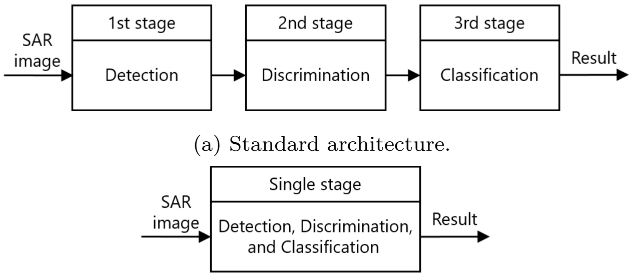

(a) Standard architecture.

(b) Proposed architecture.

Fig. 2 Architecture for an end-to-end SAR ATR system. The standard architecture is split into three stages. The Proposed architecture consists of a single stage.

performed. The CNN [13] and other methods [14]–[17] have been proposed for target and shadow region segmentation of a SAR image. In contrast, we proposed the CNN named Versnet [18] performs target detection, target classification, and pose estimation by segmentation.

Similarly, object detection that estimates the position, size, and target class of multi-target is also known. In object detection, the position and size are represented by bounding boxes. For object detection, CNNs [19]–[21] are proposed. Also, the CNN for object detection is applied to SAR ATR in [22].

On the other hand, we propose a CNN which simultaneously performs object detection and segmentation.

3. Proposed Method

A proposed CNN named SAR ATR with verification support (SAVERS) inputs an arbitrary size SAR image with multiple classes and multiple targets, and outputs the position, class, and shape of each detected target as a SAR ATR image.

Figure 1 shows the outline of SAVERS for end-to-end SAR ATR. SAVERS is a CNN composed of an encoder and a decoder. The encoder of SAVERS extracts features from an input SAR image. The decoder converts the features based on the conversion rule in the training data and outputs it as a SAR ATR image.

Here, we define the end-to-end SAR ATR as a task of supervised learning. Let $\{(X_n, D_n), n = 1, ..., N\}$ be the training dataset, where $X_n = \{x_i^{(n)}, i = 1, ..., |X_n|\}$ is SAR image as input data, $D_n = \{d_i^{(n)}, i = 1, ..., |D_n|, d_i^{(n)} \in \{0, ..., N_c - 1\}\}$ is label image for X_n, which is the supervised data of SAVERS output data $Y_n = f(X_n; \theta)$. The values of $|X_n|$ and $|D_n|$ represent the number of pixels (vertical × horizontal) of SAR and label image, respectively. When $d_i^{(n)}$ is 0, it represents a background class, and when $d_i^{(n)}$ is 1 or more, it indicates a corresponding target class. Let $L(\theta)$ be a loss function, the network parameters θ are adjusted using training data so that the output of loss function becomes small.

4. Experiments

4.1 Dataset

For training and testing of SAVERS, we used the 11 classes data shown in Table 1. The image chips have ten target classes and a background (i.e. non-target) class.

The data of ten target classes contains 2747 target chips with a depression angle of 17° for the training and 2420 target chips with a depression angle of 15° for the testing from the MSTAR [5] dataset. Five target chips of target class BTR60 for testing data were excluded. Table 2 shows a list of target chips excluded from testing data.

The data of a background class contains 274 and 242 clutter chips for the training and testing, respectively. We use clutter chips provided by Adaptive SAR ATR Problem Set (AdaptSAPS) [23] using the MSTAR dataset.

Of course, label images for segmentation do not exist in the MSTAR dataset. Therefore, we create label images for SAVERS. Figure 4d shows samples of label images. The label images have all 11 classes: 10 target classes and a background (i.e. non-target) class.

4.2 SAVERS: Proposed CNN

Figure 5 shows a detailed architecture of SAVERS for ex-

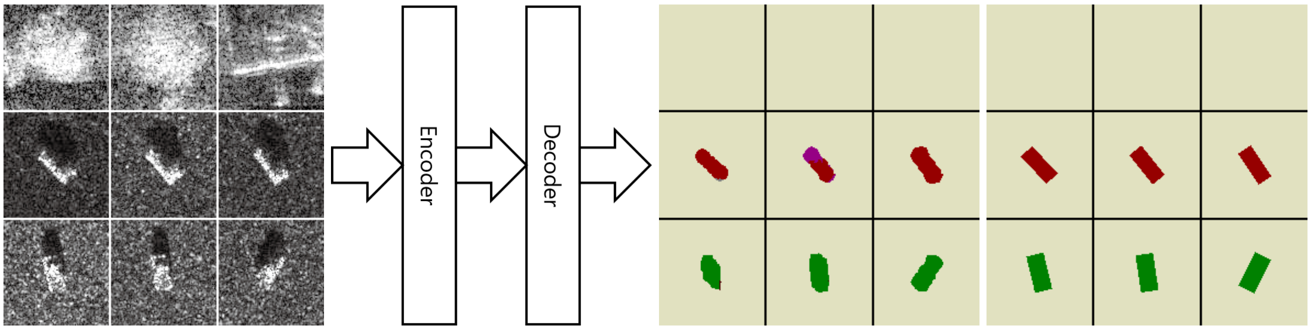

(a) Input data X_n. (b) SAVERS. (c) Output data Y_n. (d) Supervised data D_n.

Fig. 4 Illustration of training for proposed CNN.

Table 1 Dataset. The training and testing data contain respectively 3021 and 2662 image chips.

Class	Training data	Testing data
Background	274	242
2S1	299	274
BMP2 (9563)	233	195
BRDM2	298	274
BTR60	256	190
BTR70	233	196
D7	299	274
T62	299	273
T72 (132)	232	196
ZIL131	299	274
ZSU234	299	274
Total	3021	2662

Table 2 List of target chips excluded from testing data.

Class	Filename	Aspect angle (°)
BTR60	HB03353.003	305.48
BTR60	HB04933.003	303.48
BTR60	HB04999.003	299.48
BTR60	HB05000.003	304.48
BTR60	HB05631.003	302.48

periments. The encoder of the SAVERS consists of four convolution blocks and two convolution layers. The convolution block contains two convolution layers of kernel size 3×3 and a max pooling layer similarly to VGG [24]. The activation function of all convolutions except the final convolution uses rectified linear unit (ReLU) [25]. Dropout [26] is applied after a convolution of kernel size 4×4. Batch normalization [27] is not applied. The decoder of the SAVERS consists of a transposed convolution [28] that performs 16 times upsampling.

As the loss function, we use cross entropy expressed by

$$L(\theta) = -\sum_{x} p(x) \log q(x). \qquad (1)$$

For the optimization of the loss function, we use stochastic gradient descent (SGD) with momentum.

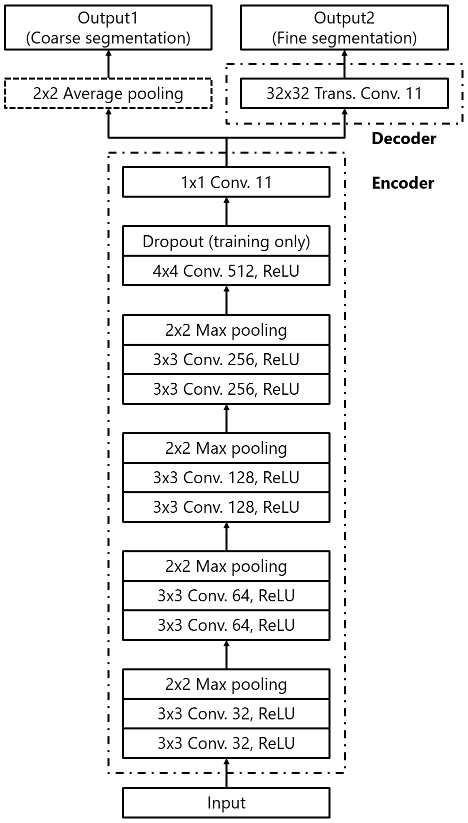

Fig. 5 Detail architecture of SAVERS for experiments. The SAVERS refers to the fully convolutional network called FCN-32s.

Since the SAVERS is a CNN without fully connected layers called fully convolutional network (FCN) [10], even if training is done with small size images, the SAVERS can process SAR images of arbitrary size.

4.3 Coarse Segmentation

First, we show results of coarse segmentation.

The decoder output performs pixel-wise segmentation (i.e. fine segmentation), whereas the encoder output is used for region-wise segmentation (i.e. coarse segmentation).

Figure 6a shows class accuracy using the encoder output before the average pooling layer. We simply use the maximum probability class (i.e. $\arg\max(p)$) as predicted class. The class accuracy before average pooling is high in the four

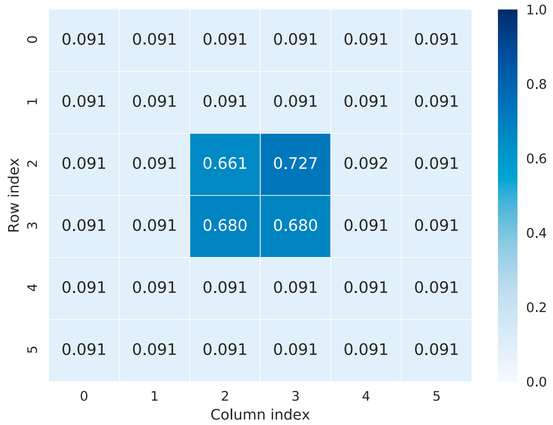

(a) Before average pooling.

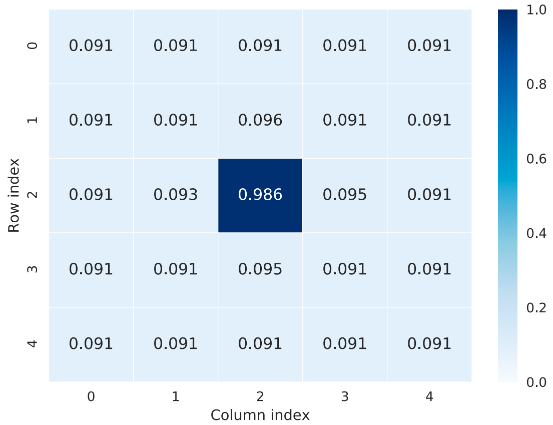

(b) After average pooling.

Fig. 6 Classification accuracy of coarse segmentation.

areas near the center, but its value is 0.661 to 0.727. The class accuracy of the peripheral area is 0.091 (242/2662) because the clutter chips are correctly classified as background class.

Figure 6b shows class accuracy using the encoder output after the average pooling layer. By performing an average pooling, the scores dispersed in the four regions are aggregated, and the class accuracy of the central region is increased to 0.986 (2624/2662).

4.4 Classification Performance of Coarse Segmentation

Next, we show results of classification performance of coarse segmentation output (i.e. the encoder output after the average pooling layer).

We use precision, recall, and F_1 as metrics of classification performance. Each metrics is given by

$$\text{Precision} = \frac{\text{TP}}{\text{TP} + \text{FP}}, \tag{2}$$

$$\text{Recall} = \frac{\text{TP}}{\text{TP} + \text{FN}}, \tag{3}$$

$$F_1 = 2 \cdot \frac{\text{precision} \cdot \text{recall}}{\text{precision} + \text{recall}}, \tag{4}$$

Table 3 Definitions of TP, FP, FN, and TN.

Predicted \ True	Condition positive	Condition negative
Condition positive	True positive (TP)	False positive (FP)
Condition negative	False negative (FN)	True negative (TN)

Table 4 Classification performance of testing.

Class	Precision	Recall	F_1
Background	0.903	1.000	0.949
2S1	0.986	0.993	0.989
BMP2	1.000	0.995	0.997
BRDM2	1.000	0.978	0.989
BTR60	1.000	0.974	0.987
BTR70	1.000	0.990	0.995
D7	1.000	0.960	0.980
T62	0.989	0.985	0.987
T72	0.995	1.000	0.997
ZIL131	0.993	0.978	0.985
ZSU234	0.993	0.996	0.995

where the definitions of TP, FP, FN, and TN are shown in Table 3.

Table 4 shows precision, recall, and F_1 of testing. Since all clutter chips are correctly classified as background (i.e. non-target) class, the recall is 1.000. However, because the part of the target chips is erroneously classified as background class, the precision becomes 0.903, and F_1 which is the harmonic average of precision and recall is 0.949.

Table 5 shows a confusion matrix for the image chips of testing. Each column in the confusion matrix represents the actual class, and each row represents the class predicted by the SAVERS.

Figure 7a shows a histogram of $(1 - p_0)$ for target and clutter chips, where p_0 is probability of background class obtained by softmax function.

Figure 7b shows a cumulative distribution of $(1 - p_0)$ for target chips. The empirical cumulative distribution function $\mathrm{P}((1 - p_0) \leq 0.5)$ and $\mathrm{P}((1 - p_0) \leq 0.8)$ are about 0.01 and 0.1, respectively.

4.5 Multi-Class and Multi-Target

Finally, we show the SAVERS output for multi-class and multi-target input. Figure 8 shows input (SAR image), output (SAR ATR image), and ground truth.

5. Conclusion

In this report, we proposed a CNN based on a new architecture consisting of a single stage for end-to-end SAR ATR system, not a standard architecture consisting of three stages. Unlike conventional CNN for target classification, the CNN named SAVERS inputs SAR imagery of arbitrary sizes

Table 5 Confusion matrix of testing data.

True Predicted	Background	2S1	BMP2	BRDM2	BTR60	BTR70	D7	T62	T72	ZIL131	ZSU234	Precision
Background	242	1	0	3	3	1	11	0	0	6	1	0.903
2S1	0	272	1	1	0	1	0	1	0	0	0	0.986
BMP2	0	0	194	0	0	0	0	0	0	0	0	1.000
BRDM2	0	0	0	268	0	0	0	0	0	0	0	1.000
BTR60	0	0	0	0	185	0	0	0	0	0	0	1.000
BTR70	0	0	0	0	0	194	0	0	0	0	0	1.000
D7	0	0	0	0	0	0	263	0	0	0	0	1.000
T62	0	1	0	0	2	0	0	269	0	0	0	0.989
T72	0	0	0	0	0	0	0	1	196	0	0	0.995
ZIL131	0	0	0	2	0	0	0	0	0	268	0	0.993
ZSU234	0	0	0	0	0	0	0	2	0	0	273	0.993
Recall	1.000	0.993	0.995	0.978	0.974	0.990	0.960	0.985	1.000	0.978	0.996	
F_1	0.949	0.989	0.997	0.989	0.987	0.995	0.980	0.987	0.997	0.985	0.995	

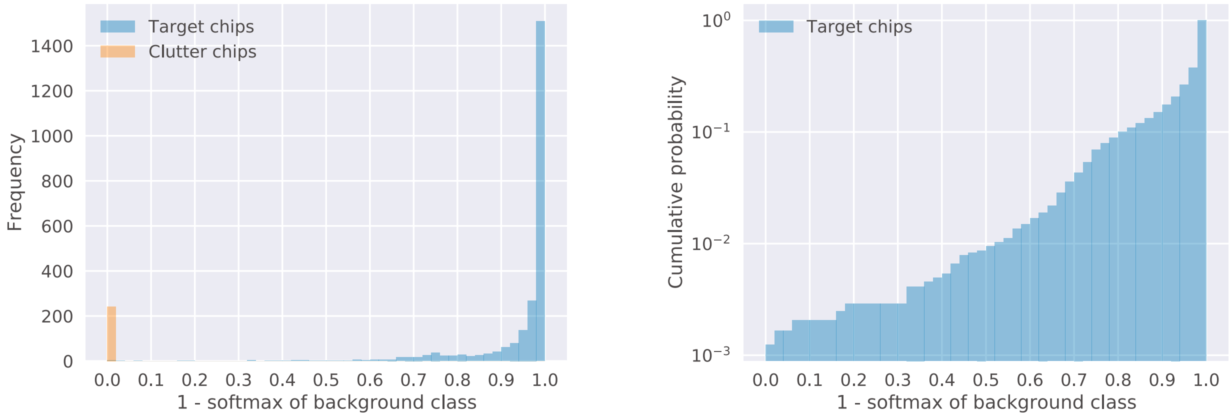

(a) Histogram.

(b) Cumulative distribution.

Fig. 7 Histogram and cumulative distribution of (1 - softmax of background class).

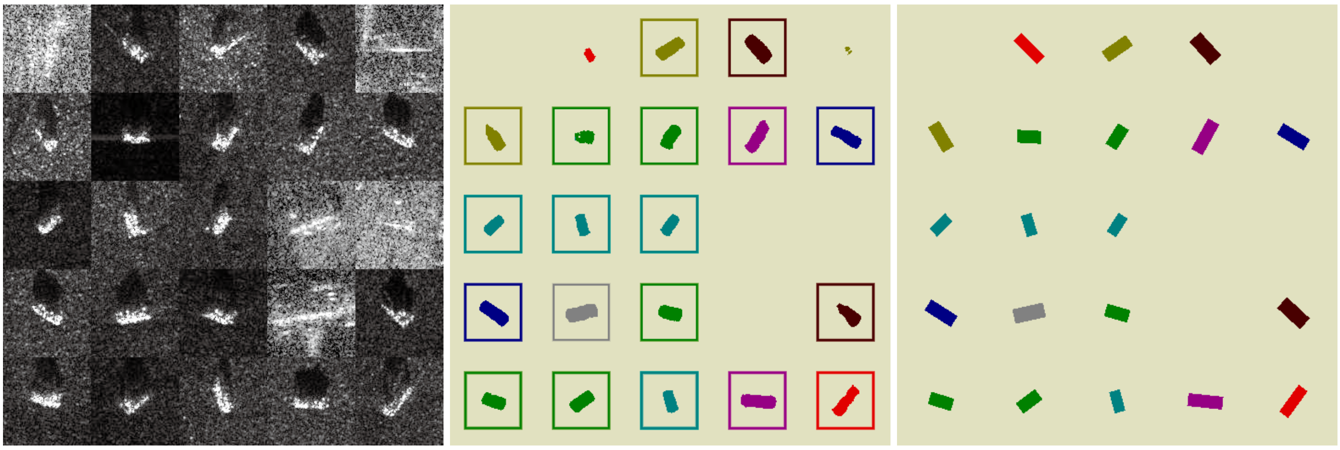

(a) Input (SAR image).

(b) Output (SAR ATR image).

(c) Ground truth.

Fig. 8 Multi-class and multi-target.

with multi-class and multi-target, discriminates between target and non-target (i.e. clutter), and output the position, class, and shape of each detected target as SAR ATR image.

We trained SAVERS to output scores of ten target classes and a background class (i.e. clutter) per pixel using the target chips of the MSTAR dataset and the clutter chips provided by AdaptSAPS, and we evaluated the performance of encoder output obtained by training. In the evaluation, the classification accuracy of the encoder output applied with average pooling was 98.6% (2624/2662).

Although this accuracy is inferior to the classification performance of state-of-the-art which classifies only the class of the target chip, it acquired the function of discrimination between target and non-target. A detailed analysis of the classification performance shows that clutter chips are correctly classified as background class, but part of the target chips are classified as background class, and extended study is future work.

References

[1] A. Krizhevsky, I. Sutskever, and G.E. Hinton, “Imagenet classification with deep convolutional neural networks,” Advances in neural information processing systems, pp.1097–1105, 2012.

[2] M.D. Zeiler and R. Fergus, “Visualizing and understanding convolutional networks,” European conference on computer vision, pp.818–833, 2014.

[3] C. Szegedy, W. Liu, Y. Jia, P. Sermanet, S. Reed, D. Anguelov, D. Erhan, V. Vanhoucke, and A. Rabinovich, “Going deeper with convolutions,” Proceedings of the IEEE conference on computer vision and pattern recognition, pp.1–9, 2015.

[4] K. He, X. Zhang, S. Ren, and J. Sun, “Deep residual learning for image recognition,” Proceedings of the IEEE conference on computer vision and pattern recognition, pp.770–778, 2016.

[5] T. Ross, S. Worrell, V. Velten, J. Mossing, and M. Bryant, “Standard sar atr evaluation experiments using the mstar public release data set,” Proc. SPIE, vol.3370, pp.566–573, 1998.

[6] S. Chen, H. Wang, F. Xu, and Y.Q. Jin, “Target classification using the deep convolutional networks for sar images,” IEEE Transactions on Geoscience and Remote Sensing, vol.54, no.8, pp.4806–4817, 2016.

[7] S. Wagner, “Sar atr by a combination of convolutional neural network and support vector machines,” IEEE Transactions on Aerospace and Electronic Systems, vol.52, no.6, pp.2861–2872, 2016.

[8] Y. Zhong and G. Ettinger, “Enlightening deep neural networks with knowledge of confounding factors,” arXiv preprint arXiv:1607.02397, 2016.

[9] H. Furukawa, “Deep learning for target classification from sar imagery: Data augmentation and translation invariance,” IEICE Tech. Rep., vol.117, no.182, SANE2017-30, pp.13-17, arXiv preprint arXiv:1708.07920, 2017.

[10] J. Long, E. Shelhamer, and T. Darrell, “Fully convolutional networks for semantic segmentation,” Proceedings of the IEEE Conference on Computer Vision and Pattern Recognition, pp.3431–3440, 2015.

[11] O. Ronneberger, P. Fischer, and T. Brox, “U-net: Convolutional networks for biomedical image segmentation,” International Conference on Medical Image Computing and Computer-Assisted Intervention, pp.234–241, 2015.

[12] V. Badrinarayanan, A. Kendall, and R. Cipolla, “Segnet: A deep convolutional encoder-decoder architecture for image segmentation,” arXiv preprint arXiv:1511.00561, 2015.

[13] D. Malmgren-Hansen and M. Nobel-J, “Convolutional neural networks for sar image segmentation,” 2015 IEEE International Symposium on Signal Processing and Information Technology (ISSPIT), pp.231–236, 2015.

[14] S. Huang and T.Z. Wenzhun Huang, “A new sar image segmentation algorithm for the detection of target and shadow regions,” Scientific reports 6, Article number: 38596, 2016.

[15] Y. Han, Y. Li, and W. Yu, “Sar target segmentation based on shape prior,” 2014 IEEE International Geoscience and Remote Sensing Symposium (IGARSS), pp.3738–3741, 2014.

[16] E. Aitnouri, S. Wang, and D. Ziou, “Segmentation of small vehicle targets in sar images,” Proc. SPIE, vol.4726, no.1, pp.35–45, 2002.

[17] R.A. Weisenseel, W.C. Karl, D.A. Castanon, G.J. Power, and P. Douville, “Markov random field segmentation methods for sar target chips,” Proc. SPIE, vol.3721, pp.462–473, 1999.

[18] H. Furukawa, “Deep learning for end-to-end automatic target recognition from synthetic aperture radar imagery,” IEICE Tech. Rep., vol.117, no.403, SANE2017-92, pp.35-40, arXiv preprint arXiv:1801.08558, 2018.

[19] R. Girshick, J. Donahue, T. Darrell, and J. Malik, “Rich feature hierarchies for accurate object detection and semantic segmentation,” Proceedings of the IEEE conference on computer vision and pattern recognition, pp.580–587, 2014.

[20] R. Girshick, “Fast r-cnn,” Proceeding of the IEEE International Conference on Computer Vision (ICCV), pp.1440–1448, 2015.

[21] S. Ren, K. He, R. Girshick, and J. Sun, “Faster r-cnn: Towards real-time object detection with region proposal networks,” Advances in neural information processing systems, pp.91–99, 2015.

[22] S. Wang, Z. Cui, and Z. Cao, “Target recognition in large scene sar images based on region proposal regression,” Geoscience and Remote Sensing Symposium (IGARSS), 2017 IEEE International, pp.3297–3300, 2017.

[23] A.R. Wise, D. Fitzgerald, and T.D. Ross, “Adaptive sar atr problem set (adaptsaps),” Algorithms for Synthetic Aperture Radar Imagery XI, vol.5427, pp.366–376, 2004.

[24] K. Simonyan and A. Zisserman, “Very deep convolutional networks for large-scale image recognition,” arXiv preprint arXiv:1409.1556, 2014.

[25] V. Nair and G.E. Hinton, “Rectified linear units improve restricted boltzmann machines,” Proceedings of the 27th international conference on machine learning (ICML-10), pp.807–814, 2010.

[26] N. Srivastava, G.E. Hinton, A. Krizhevsky, I. Sutskever, and R. Salakhutdinov, “Dropout: a simple way to prevent neural networks from overfitting.,” Journal of Machine Learning Research, vol.15, no.1, pp.1929–1958, 2014.

[27] S. Ioffe and C. Szegedy, “Batch normalization: Accelerating deep network training by reducing internal covariate shift,” International Conference on Machine Learning, pp.448–456, 2015.

[28] V. Dumoulin and F. Visin, “A guide to convolution arithmetic for deep learning,” arXiv preprint arXiv:1603.07285, 2016.